ISJ 21: 179-192, 2024 ISSN 1824-307X

RESEARCH REPORT

Histopathological characterization of *Penaeus vannamei* experimentally infected with *Vibrio parahaemolyticus* causing acute hepatopancreatic necrosis disease

Y Gu[1,2], P Ni[2,3], M-Q Wang[1,2,3,4,5]*

[1]*Southern Marine Science and Engineering Guangdong Laboratory (Guangzhou), Guangzhou 511458, China*
[2]*Hainan Key Laboratory of Tropical Aquatic Germplasm, Sanya Oceanographic Institution, Ocean University of China, Sanya 572024, China*
[3]*MOE Key Laboratory of Marine Genetics and Breeding, Ocean University of China, Qingdao 266003, China*
[4]*Shandong Key Laboratory of Marine Seed Industry (preparatory), Ocean University of China, Qingdao 266003, China*
[5]*Qingdao Institute of Maritime Silk Road (Qingdao Institute of Blue Seed Industry), Ocean University of China, Qingdao 266073, China*

 Accepted December 15, 2024

Abstract

Vibrio parahaemolyticus carrying the *pirA* and *pirB* gene is one of the major pathogens causing acute hepatopancreatic necrosis disease (AHPND) in shrimp. It primarily targets the hepatopancreas as target tissue, causing pathological damage by releasing binary toxins during intestinal colonization. In this study, *Penaeus vannamei* were infected with *V. parahaemolyticus* causing acute hepatopancreatic necrosis disease (*Vp*^{AHPND}), and tissue samples were collected from surviving, moribund, and dead shrimps, including gills, heart, stomach, hepatopancreas, muscle, midgut, hindgut, and pleopod. The relationship between bacterial loads and pathological damage in the infected shrimp tissues was identified using real-time PCR (qPCR) combined with histopathology. The qPCR results showed that *V. parahaemolyticus* was detectable in all tissue samples, with the highest positivity rate in the hepatopancreas at 94.44%, and the lowest in muscles at 44.44%. The hepatopancreas is highly sensitive tissues for AHPND detection, sequentially followed by pleopod and gill. Histopathological analysis revealed that *Vp*^{AHPND} infection caused varying degrees of damage to the morphology of tissues such as shrimp gills, stomach, hepatopancreas, midgut, hindgut, and pleopods. By analyzing the pathological characteristics of infected tissues with different bacterial load levels, a high correlation was found between the load of *V. parahaemolyticus* in each tissue and the degree of infection. This study can help to understand the pathogenic mechanism of *Vibrio parahaemolyticus* infection in shrimp, assess the degree of infection, and evaluate the progress of the disease.

Key Words: acute hepatopancreatic necrosis disease; histopathological analysis; *Penaeus vannamei*; *Vibrio parahaemolyticus*

Introduction

Shrimps dominate the aquaculture industry, accounting for over 65% of production (Hu *et al*., 2024). *Penaeus vannamei* is a widely cultivated shrimp species, and plays an important role in providing aquatic proteins (Lee *et al*., 2022). However, with the continuous development of global aquaculture industry, shrimp farming faces severe disease challenges due to environmental pollution, high density, and other factors. Bacterial diseases have caused serious damage and economic losses to the shrimp farming industry (de la Peña *et al*., 2015; Dhar *et al*., 2019). One of the major bacterial pathogens causing acute hepatopancreatic necrosis disease (AHPND) in shrimp is the pathogenic *V. parahaemolyticus* (*Vp*^{AHPND}) carrying the pVA-1 plasmid encoding pirA and pirB toxins (Tran *et al*., 2013; Nunan *et al*., 2014). To date, the pathogenesis of *Vp*^{AHPND} in shrimp have not yet been fully elucidated, specifically regarding its spread within the shrimp and the resulting tissue damage.

At the molecular mechanism level, the discovery of the pVA1 plasmid carried by *Vp*^{AHPND} is a milestone, and the binary pirA/B toxins are considered as key diagnostic markers for AHPND

Corresponding author:
Mengqiang Wang
Southern Marine Science and
Engineering Guangdong Laboratory (Guangzhou)
Guangzhou 511458, China
E-mail: wangmengqiang@ouc.edu.cn

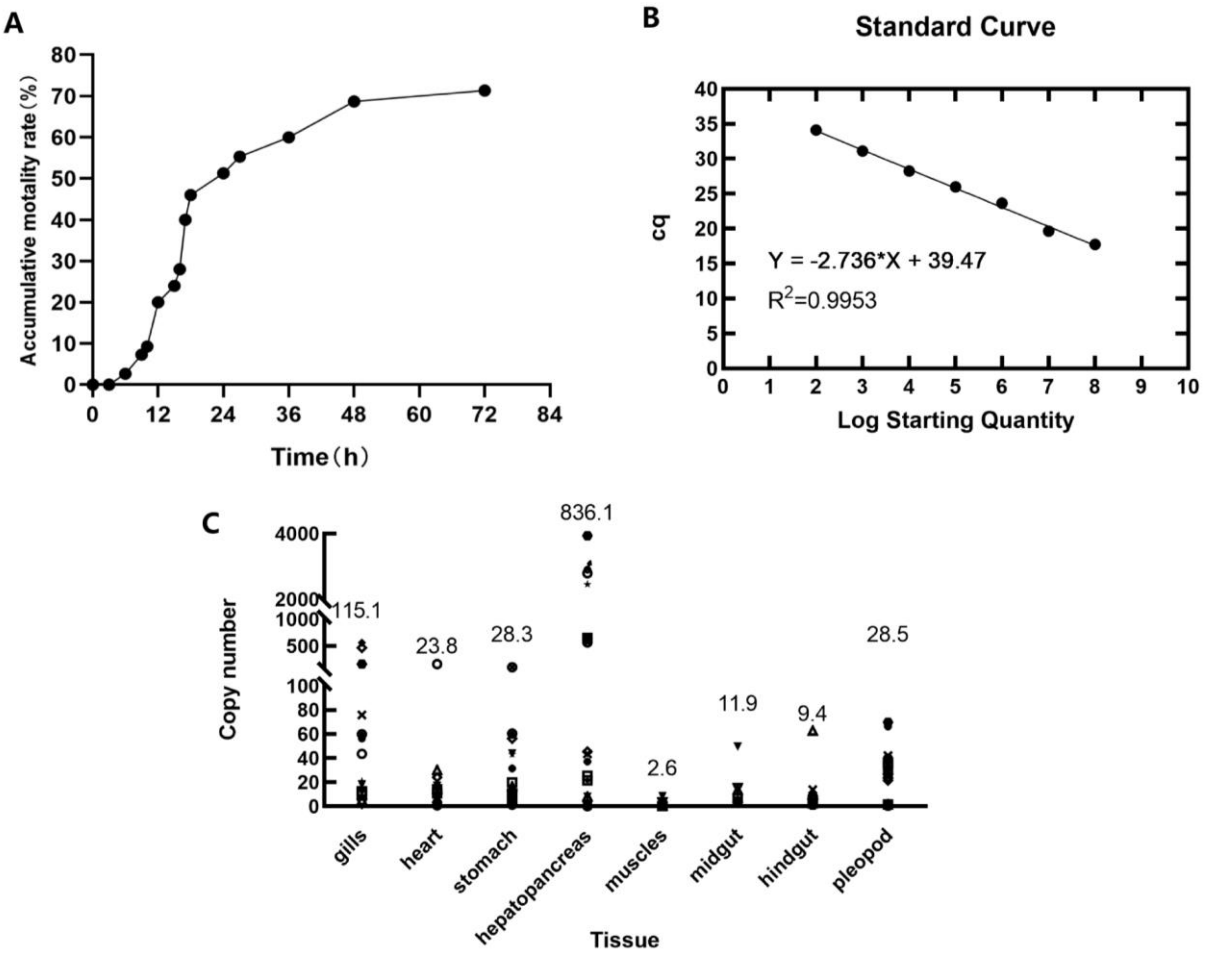

Fig. 1 The infection and detection of *Vp*^{AHPND} in shrimps. (A) The cumulative mortality rate of shrimp infected with *Vp*^{AHPND}. (B) The standard curve of pirA/B in qPCR detection. (C) The bacterial load in various tissues of shrimp infected with *Vp*^{AHPND}

(Lee *et al*., 2015). Based on this, researchers have developed a series of PCR methods targeting to specific sequences of the plasmid, greatly advancing the diagnostic technology for AHPND (Dangtip *et al*., 2015; Han *et al*., 2015a; Kongrueng *et al*., 2015; Cruz-Flores *et al*., 2019). Histopathology is a common way to study disease. Previous studies showed that *V. parahaemolyticus* causing AHPND primarily affects the digestive gland of shrimp, especially the hepatopancreas. This infection leads to pale atrophy of the hepatopancreas, empty stomach and intestines, shedding of epithelial cells in the hepatopancreatic tubules, enlargement of cell nuclei, deformation of stellar cavities, and loss of functional cells. During the infection progresses, necrosis occurs in the hepatopancreatic tubules, hemocyte infiltration triggers an inflammatory response, and nodules are formed. It is insufficient to rely solely on changes in the hepatopancreas to diagnose AHPND, and these clinical features of AHPND can also be present in some other diseases (Hong et al., 2016). However, little information was available on the histopathology of AHPND yet.

A previous study found that *P. vannamei* exhibited significant physiological changes at 6 hours after being infected with *V. parahaemolyticus*, the pathogen was detectable in the gills, hepatopancreas, intestines, muscles, and hemolymph, and the pathogen would continue to cause pathological damage to the tissues (Khimmakthong and Sukkarun, 2017). A pathobiological study on *P. vannamei* infected with *V. parahaemolyticus* observed varying degrees of lesions in the epidermis, skeletal structures, cardiac muscle, hepatopancreas tubules, stomach, and the lumen of intestine (Ananda Raja *et al*., 2017). *V. parahaemolyticus* can elicit systemic responses in the host (Li *et al*., 2023), and penetrate the epithelial tissue of shrimp and establish an infection through various routes of exposure, such as damaged tissues, gills, oral cavity, or feed (Martin *et al*., 2004). The infection of bacteria often affects multiple tissues of shrimp, and it may cause a series of pathological damage and immune responses in the host during the process from invasion to reproduction. Therefore, understanding

Table 1 The qPCR results of tissue samples from the experimental group

Types of shrimp	gills	heart	stomach	hepatopancreas	muscles	midgut	hindgut	pleopod
Survival shrimp	18.0	17.2	44.0	7.9	/	/	/	29.3
	/	8.0	4.2	2.4	/	/	/	32.8
	563.5	161.1	1.4	2797.4	/	/	/	/
	43.6	/	/	/	/	/	2.1	2.0
	/	14.3	19.9	25.4	/	/	5.1	1.6
	10.9	/	16.4	8.1	8.6	49.7	/	27.2
Moribund shrimp	5.3	/	10.5	1.0	/	/	/	23.0
	/	30.2	56.3	45.4	/	/	8.1	21.6
	2.3	7.1	/	37.2	/	5.4	2.4	66.2
	465.5	24.1	31.4	2457.4	/	/	/	/
	/	/	/	3938.3	2.7	4.3	62.9	1.5
	56.3	2.9	43.2	43.5	1.4	6.7	/	69.9
Dead shrimp	20.6	15.9	2.2	0.1	0.2	13.6	2.2	42.1
	161.9	3.4	13.9	21.6	0.8	15.2	6.7	0.5
	/	13.1	60.4	567.8	3.4	3.3	1.1	35.8
	75.8	/	10.3	648.3	/	1.9	0.6	28.6
	59.9	0.9	103.8	631.1	3.1	6.6	1.0	34.2
	12.6	10.9	6.8	2980.9	1.0	/	13.9	40.0

the characteristic information of histopathological changes after infection with *V. parahaemolyticus* causing AHPND could be helpful in the early pathogen diagnosis of AHPND, assessing the extent of the disease, and formulating preventive and control measures.

In this study, we utilized a combination of molecular biology detection method and histopathological technique to investigate the transmission of *V. parahaemolyticus* in *P. vannamei* and to examine the pathological process and damage associated with AHPND. By examining different tissues of the shrimp exposed to *V. parahaemolyticus*, our findings will also contribute to a better understanding of the pathological mechanisms underlying AHPND.

Materials and Methods

Shrimp and Pathogens

The shrimps used in this experiment were obtained from a farm in Lingao, Hainan, with an average weight of 10 ± 0.1 g and an average length of 7 ± 0.1 cm. Before the experiment, we detected the main pathogens of shrimp, including covert mortality nodavirus (Xu *et al*., 2023), Decapod iridescent virus 1 (Xu *et al*., 2022), *Enterocytozoon hepatopanaei* (Li *et al*., 2023), infectious myonecrosis virus (Zhang *et al*., 2024b), infectious hypodermal and hematopoietic necrosis virus (Zhang *et al*., 2023a), Taura syndrome virus (Li *et al*., 2024), *Vp*AHPND (Liu *et al*., 2024), white spot syndrome virus (Zhang *et al*., 2023b), yellow head virus (Zhang *et al*., 2024a), to confirm the health status of the shrimp. They were temporarily cultured in the laboratory, with a temperature of 26 ± 1 °C, pH 8.0 ± 0.2, salinity of 20‰, and maintained with oxygen circulation. The seawater was exchanged by one-third every 12 h, and normal feeding was maintained for one week before subsequent infection experiments.

The Vp^{AHPND} used in the infection experiment was provided by Professor Lei Wang, Institute of Oceanology, Chinese Academy of Sciences. Before the experiment, PCR detection method was used to confirm *V. parahaemolyticus* carries the pathogenicity-related *pirA/B* gene of AHPND with the primers 5'-AGTAACAATATAAAACATGAAACTGACTATTC-3' and 5'-CTACTTTTCTGTACCAAATTCATCGG-3 according to the previous report (Zhou *et al*., 2023). The pathogenic strain Vp^{AHPND} was cultured in 2216E media (M016, HopeBio, China) and incubated in a shaker (150 rpm) at 28 °C for 20 h prior to the challenge. A bacterial suspension was harvested and washed 3 times with sterilized phosphate-buffered saline (PBS) by centrifugation at 4000 rpm for 10 min. Then suspension was diluted with sterile seawater to make a test solution of 1.0×10^7 colony-forming units (CFU) mL^{-1} for the Vp^{AHPND} stimulation.

Vp^{AHPND} stimulation and sample collection

A total of 400 healthy shrimps used in the experiment were randomly divided into two groups, experimental and control groups, with 200 individuals in each group. Then the immersion experiment was performed as previously described

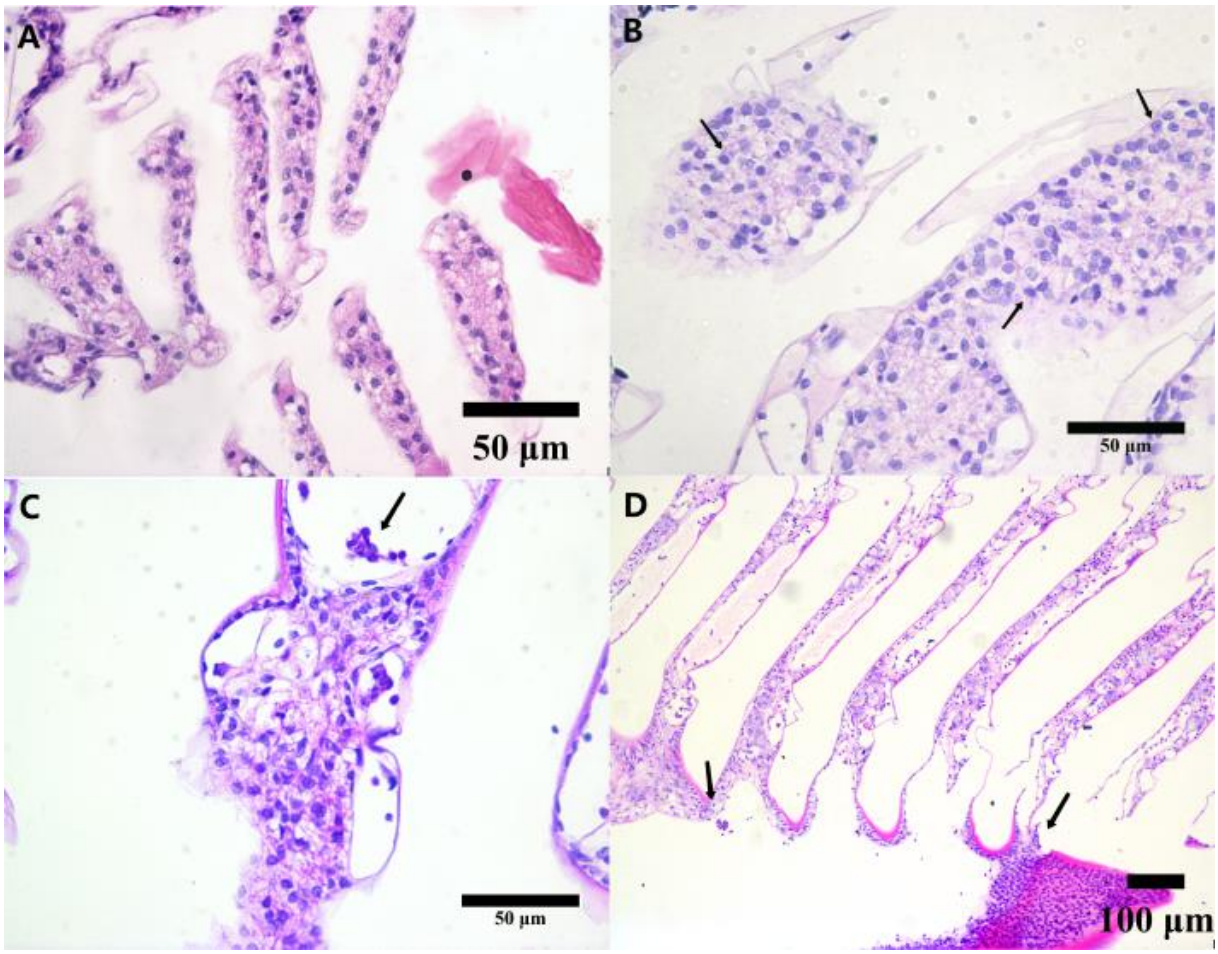

Fig. 2 Pathological sections of gill of *P. vannamei*. (A) Normal gill of shrimp. (B) shows the loads of *V. parahaemolyticus* were 5.3 copies/ng of gill. (C) shows the loads of *V. parahaemolyticus* were 59.9 copies/ng of gill. (D) shows the loads of *V. parahaemolyticus* were 465.5 copies/ng of gill. The arrow refers to the cell or tissue lesions described

(Tran *et al*., 2013). Briefly, shrimps in the experimental group were first soaked in a high concentration of bacterial solution (1.0×10^9 CFU/mL) for 15 min, and then continued to be reared in seawater with a bacterial concentration of 1.0×10^7 CFU/mL. The shrimps in the control group were not treated. When the cumulative mortality rate of shrimp in the experimental group reached 50%, six shrimp were collected from the control group, while six dead shrimp, six moribund shrimp, and six surviving shrimp were collected from the experimental group. Among them, the clinical manifestations of shrimp were defined as moribund shrimp when they showed benthic or side-lying postures, had obvious responses to external stimuli, but their gills were still slightly active. The surviving shrimp were defined as vigorous, actively swimming, and having intense responses to external stimuli. The gills, heart, stomach, hepatopancreas, muscle, midgut, hindgut, and pleopod of each shrimp were collected. All tissue samples were prepared in duplicates: one for DNA extraction and the other for histopathological examination.

The construction of standard plasmid and standard curve

The genomic DNA of *V. parahaemolyticus* was extracted using the bacterial and tissue DNA rapid extraction kit (DP324, Tiangen, China). The pirA/B gene of Vp^{AHPND} was amplified by PCR. The forward primer sequences are 5'-AGTAACAATATAAAACATGAAACTGACTATTC-3' and the reverse primer sequences are 5'-CTACTTTTTCTGTACCAAATTCATCGG-3'. The PCR products were purified using the gel extraction kit (EG101, TransGen, China), cloned into the pEASY-Blunt zero vector (CB501, TransGen, China), and then transformed into competent Trans1-T1 phage resistant chemically competent cells (CB501, TransGen, China). The positive recombinants were identified through anti-ampicillin selection, and three to five independent clones of each amplicon were sequenced. According to the manufacturer's protocol, the positive plasmids were extracted using the EasyPure HiPure plasmid MiniPrep kit (EM111, TransGen, China). The concentration of recombinant

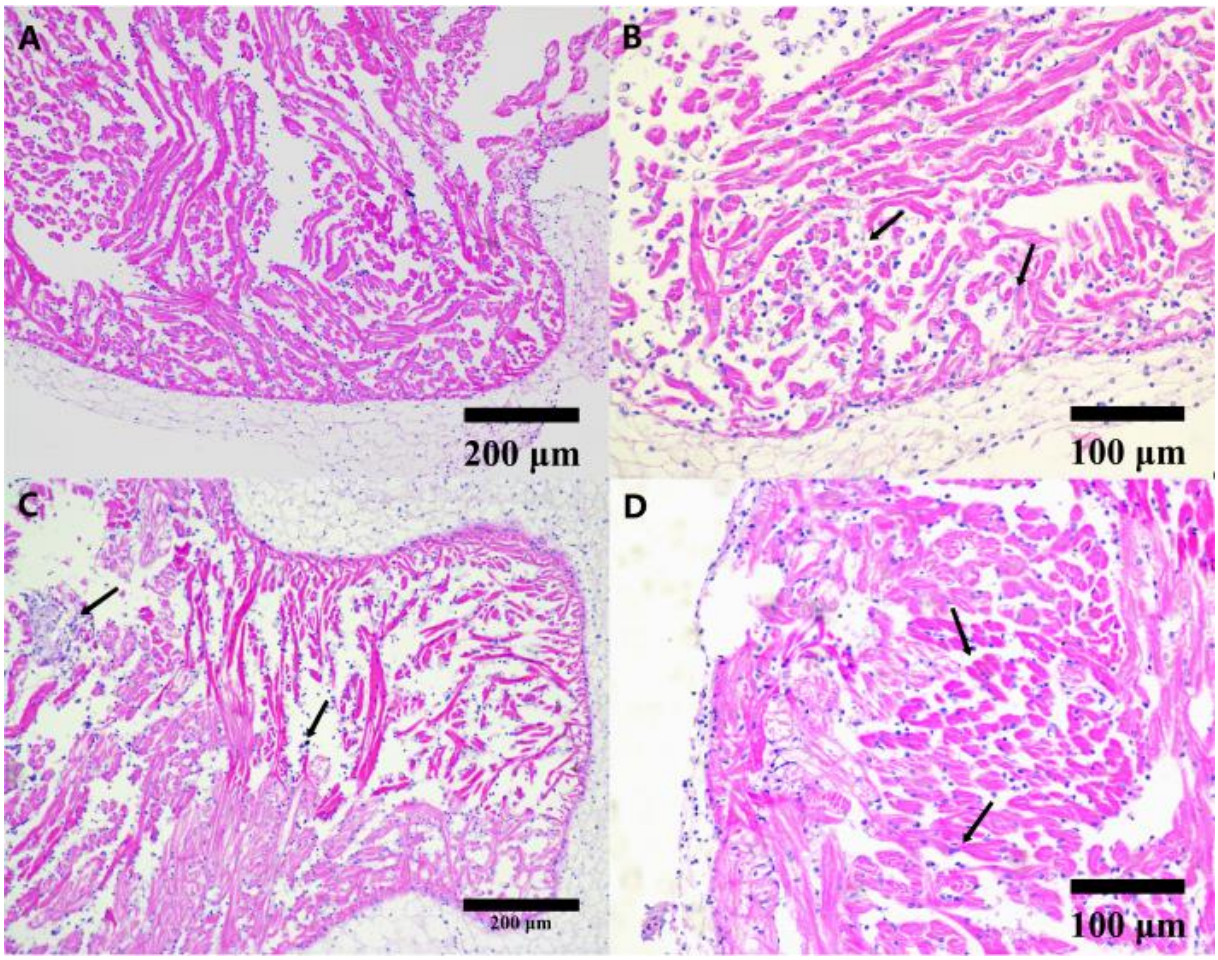

Fig. 3 Pathological sections of heart of *P. vannamei.* (A) Normal heart of shrimp. (B) shows the loads of *V. parahaemolyticus* were 0.9 copies/ng of gill. (C) shows the loads of *V. parahaemolyticus* were 13.1 copies/ng of gill. (D) shows the loads of *V. parahaemolyticus* were 161.1 copies/ng of gill. The arrow refers to the cell or tissue lesions described

plasmid was determined by measuring the ultraviolet absorbance at 260 nm and was converted to the number of plasmid DNA copies. The formula for calculating the copy number of recombinant plasmids is: Copy Number (Copies/µL) = [DNA concentration (ng/µL) × 6.02 × 10^{14}] / [length of plasmid vector (bp) × 660] (Zhang *et al*., 2009). A series of diluted plasmid DNA (10^8 - 10^2 copies/ng) were used as a calibrator, and a standard curve for quantification was generated using real-time PCR. The forward primer sequences are 5'-TTGGACTGTCGAACCAAACG-3' and the Reverse primer sequences are 5'-GCACCC1CATTGGTATTGAATG-3', and the probe is 6FAM-AGACAGCAAACATACACCTATCATCCCGGA-TAMRA. The 20 µL system consists of 0.6 µL forward primer (10 µM), 0.6 µL reverse primer (10 µM), 0.2 µL probe (10 µM), 0.8 µL DNA template, 7.8 µL ddH_2O and 10 µL premix Ex Taq (RR390A, TaKaRa, China). The pirA/B gene was amplified for 40 cycles at 95 °C for 3 s and 60 °C for 30 s. The cycling was initiated at 95 °C for 20 s. Three parallel experiments were set up, and the average Quantification Cycle (Cq) values from the three experiments were used to generate a standard regression line.

Detection and quantitation of Vp^{AHPND} in tissues

DNA was extracted from shrimp gills, heart, stomach, hepatopancreas, muscle, midgut, hindgut, and pleopods using the TIANamp marine animal DNA kit (DP324, Tiangen, China). The DNA was then diluted to 100 ng/µL and used for qPCR amplification. The qPCR system and procedures were consistent with those described. The number of DNA copies of Vp^{AHPND} per microliter of DNA is calculated from the Cq value and the above formula.

Histopathological study of Vp^{AHPND} infection in P. vannamei

The tissue samples were used for preparing conventional histopathological sections. The collected tissues were fixed in 4% paraformaldehyde for 24 h, followed by dehydration

with a series of ethanol concentrations ranging from 75% to 100% to eliminate residual water in the tissue. After dehydration, the tissues were cleared using xylene. The tissues were then infiltrated with paraffin wax using an automated tissue processor. Once the tissues were embedded in paraffin wax, it was sectioned using a microtome, resulting in sections with a thickness of 4-6 micrometers. To visualize the cellular structures within the tissue sections, hematoxylin and eosin staining (HE staining) was performed according to the conventional histological methods previously described (Lightner *et al*., 1996). After being stained, the tissue sections were dehydrated again using increasing concentrations of ethanol and cleared once more with xylene. Finally, we sealed the sections with neutral glue and observed them under an optical microscope. And we captured digital images of the stained sections using a camera attached to the microscope for further analysis.

Result

The cumulative mortality rate of shrimps

During the experiment, we continuously recorded the cumulative mortality of shrimps (Figure 1A). We found that the first death of shrimp in the experimental group occurred at 6 hours after Vp^{AHPND} stimulation, and the number of deaths began to increase significantly at 12 h. A significant clustered outbreak of deaths occurred between 12 - 24 h, with a cumulative mortality rate of approximately 50% at 24 h. From 24 h onwards, the number of deaths gradually decreased, and by 48 h, the mortality rate became very slow. In addition, we observed that some shrimps showed typical symptoms and pathological damage of AHPND, such as lethargy, slow movement, empty intestines, pale or watery hepatopancreas, and enlarged external pigmentation. The results indicated that the shrimp were successfully infected with Vp^{AHPND}.

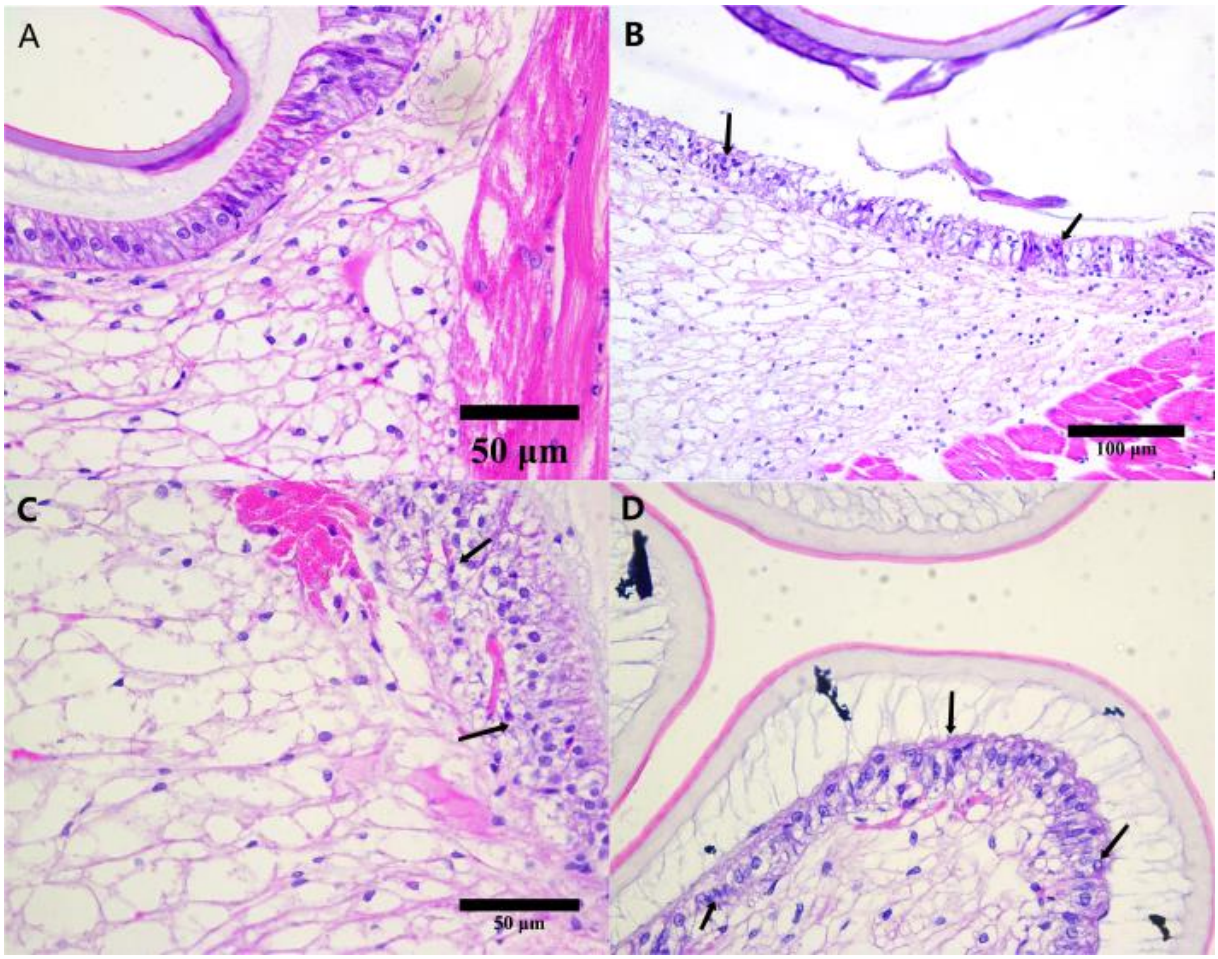

Fig. 4 Pathological sections of stomach of *P. vannamei.* (A) Normal stomach of shrimp. (B) shows the loads of *V. parahaemolyticus* were 4.2 copies/ng of stomach. (C) shows the loads of *V. parahaemolyticus* were 13.9 copies/ng of stomach. (D) shows the loads of *V. parahaemolyticus* were 60.4 copies/ng of stomach. The arrow refers to the cell or tissue lesions described

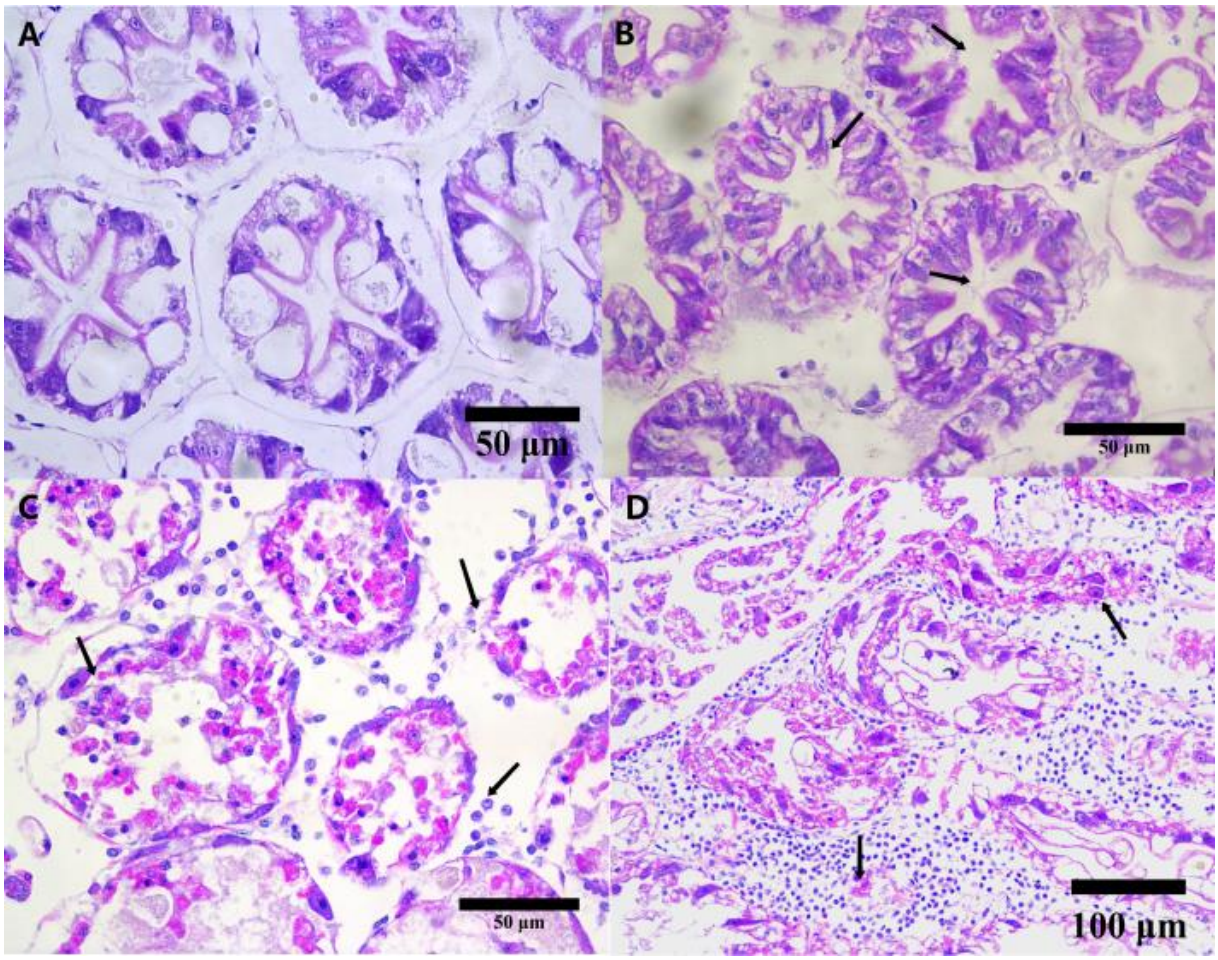

Fig. 5 Pathological sections of hepatopancreas of *P. vannamei.* (A) Normal hepatopancreas of shrimp. (B) shows the loads of *V. parahaemolyticus* were 2.4 copies/ng of hepatopancreas. (C) shows the loads of *V. parahaemolyticus* were 567.8 copies/ng of gill. (D) shows the loads of *V. parahaemolyticus* were 3938 copies/ng of hepatopancreas. The arrow refers to the cell or tissue lesions described

all results were negative (Table 1). In the experimental group, we observed that 17 out of 18 shrimp samples showed positive reactions in the hepatopancreas, with a *Vp*^{AHPND} positivity rate of 94.44%. In addition, we also observed positive reactions in 16 of pleopods, 15 of stomachs, 13 of hearts and gills, as well as 11 of midgut and 10 of hindgut. Among the muscle samples, 8 sets showed positive reactions, with a positivity rate of only 44.44%, including 5 sets from dead shrimps. Among all the positive tissue samples, the highest bacterial loads were observed in the hepatopancreas with an average of 836.1 copies/ng (Figure 1C). The average bacterial loads in the gills were 115.1 copies/ng, while that in the pleopods was 28.5 copies/ng, and in the stomach were 28.3 copies/ng. The average bacterial loads in the heart were 23.8 copies/ng. The average bacterial counts for the midgut and hindgut were 11.9 copies/ng and 9.4 copies/ng respectively. The lowest average bacterial loads were observed in the muscle, which were only 2.6 copies/ng.

Histopathological study of VpAHPND infection in P. vannamei

Pathological changes of gills tissue

In the healthy shrimp, the gills presented a typical branch-like structure, consisting of the main gill axis and numerous closely arranged gill filaments (Figure 2A). In diseased shrimps, significant swelling of the nuclei in some gill filament cells was observed, along with sporadically distributed necrotic cells, indicating that the *Vibrio* had begun to cause damage to the gill tissue (Figure 2B, 5.3 copies/ng). The interior of the gill filaments was significantly dilated and swollen, disrupting the originally orderly structure. Moreover, numerous vacuoles frequently occurred inside, and the number of necrotic cells also markedly increased (Figure 2C, 59.9 copies/ng). As the *Vibrio* load further increased, extensive necrosis of the gill filaments occurred, with their arrangement becoming highly irregular. Additionally, focal necrosis could be observed within the tissue, with a significant accumulation of necrotic tissue debris (Figure 2D, 465.5 copies/ng).

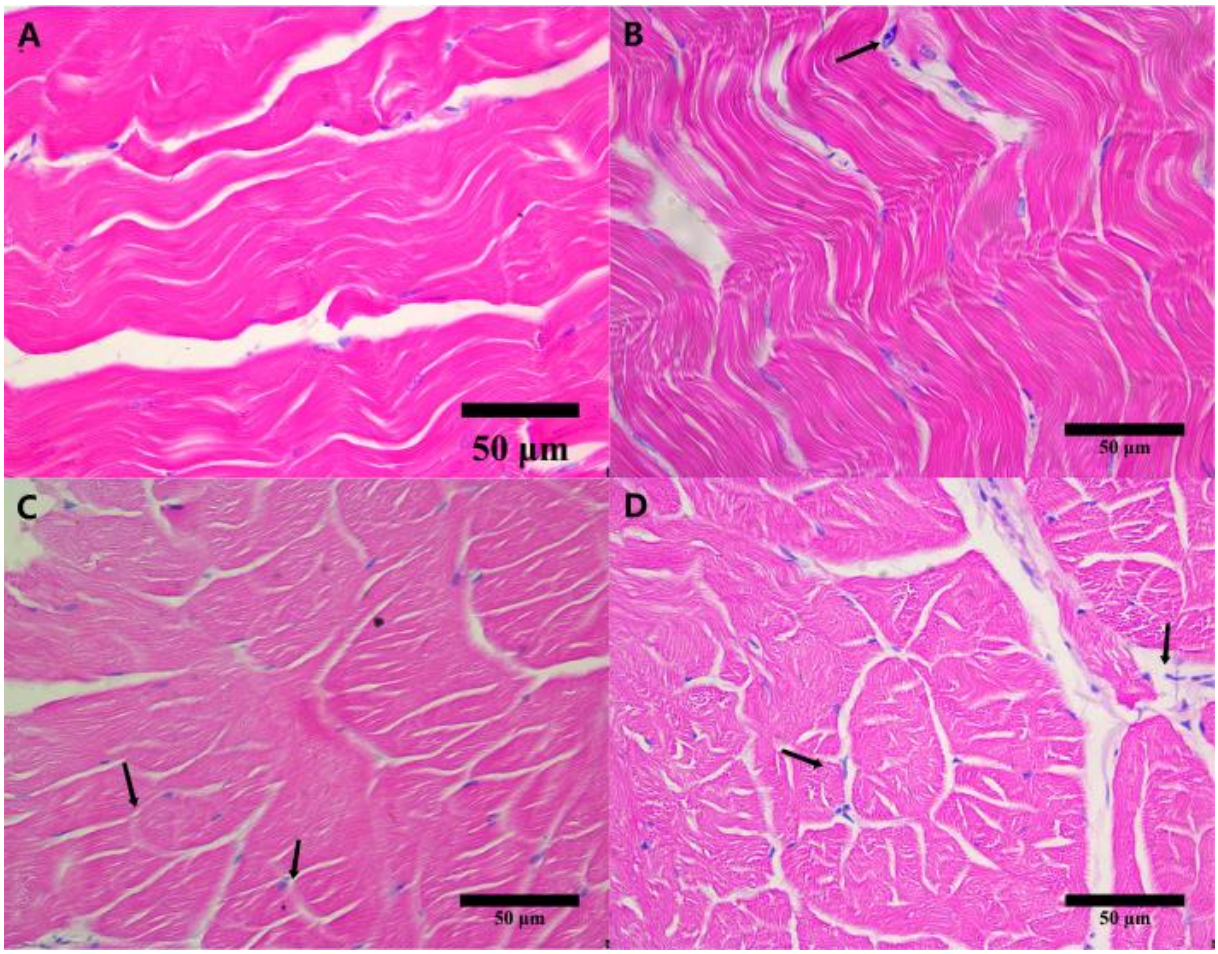

Fig. 6 Pathological sections of muscle of *P. vannamei.* (A) Normal muscle of shrimp. (B) shows the loads of *V. parahaemolyticus* were 0.2 copies/ng of muscle. (C) shows the loads of *V. parahaemolyticus* were 3.4 copies/ng of muscle. (D) shows the loads of *V. parahaemolyticus* were 8.6 copies/ng of muscle. The arrow refers to the cell or tissue lesions described

Pathological changes of heart tissue

In the healthy shrimp, the heart is composed of cardiac muscle fibers and cells, which crisscross in an orderly manner to form a complex reticular structure (Figure 3A). In diseased shrimps, the striated structure of the cardiac muscle fibers began to blur, with initial ruptures occurring and the orderly arrangement of the fibers being lost. The nuclei in some cardiac muscle cells showed swelling, with a few even appearing necrotic (Figure 3B, 0.9 copies/ng). Then, the rupture and bending of the cardiac muscle fibers worsened, making the overall structure more chaotic and disordered. The number of necrotic cardiac muscle fibers and cells significantly increased, indicating that the damage to the heart due to *Vibrio* infection was intensifying (Figure 3C, 13.1 copies/ng). As the *Vibrio* load further increased, widespread rupture of the cardiac muscle fibers occurred, forming block-like structures that lost their connections with each other. The striated structure of the cardiac muscle fibers disappeared in most areas. The necrosis between tissues became severer (Figure 3D, 161.1 copies/ng).

Pathological changes of stomach tissue

In the healthy shrimp, the stomach wall consists of the mucosa, submucosa, and muscle layers. The mucosa, as the innermost layer, includes epithelial cells, glands, and blood vessels (Figure 4A). In diseased shrimps, some of the nuclei exhibited swelling, and necrotic material accumulation along with the presence of necrotic cells was observed within the tissue. These are signs of cellular stress response and damage indicative of early-stage infection (Figure 4B, 4.2 copies/ng). Subsequently, the pathological condition of the gastric tissue worsened. The arrangement of the epithelial cells shifted from orderly to disorganized, with an increased occurrence of cell necrosis and shedding (Figure 4C, 13.9 copies/ng). With the massive proliferation of *Vibrio*, cell necrosis became widespread, and the epithelial cells exhibited significant vacuolar degeneration (Figure 4D, 60.4 copies/ng).

Pathological changes of hepatopancreas tissue

In the healthy shrimp, the hepatopancreas is composed of numerous hepatocytes, which form a

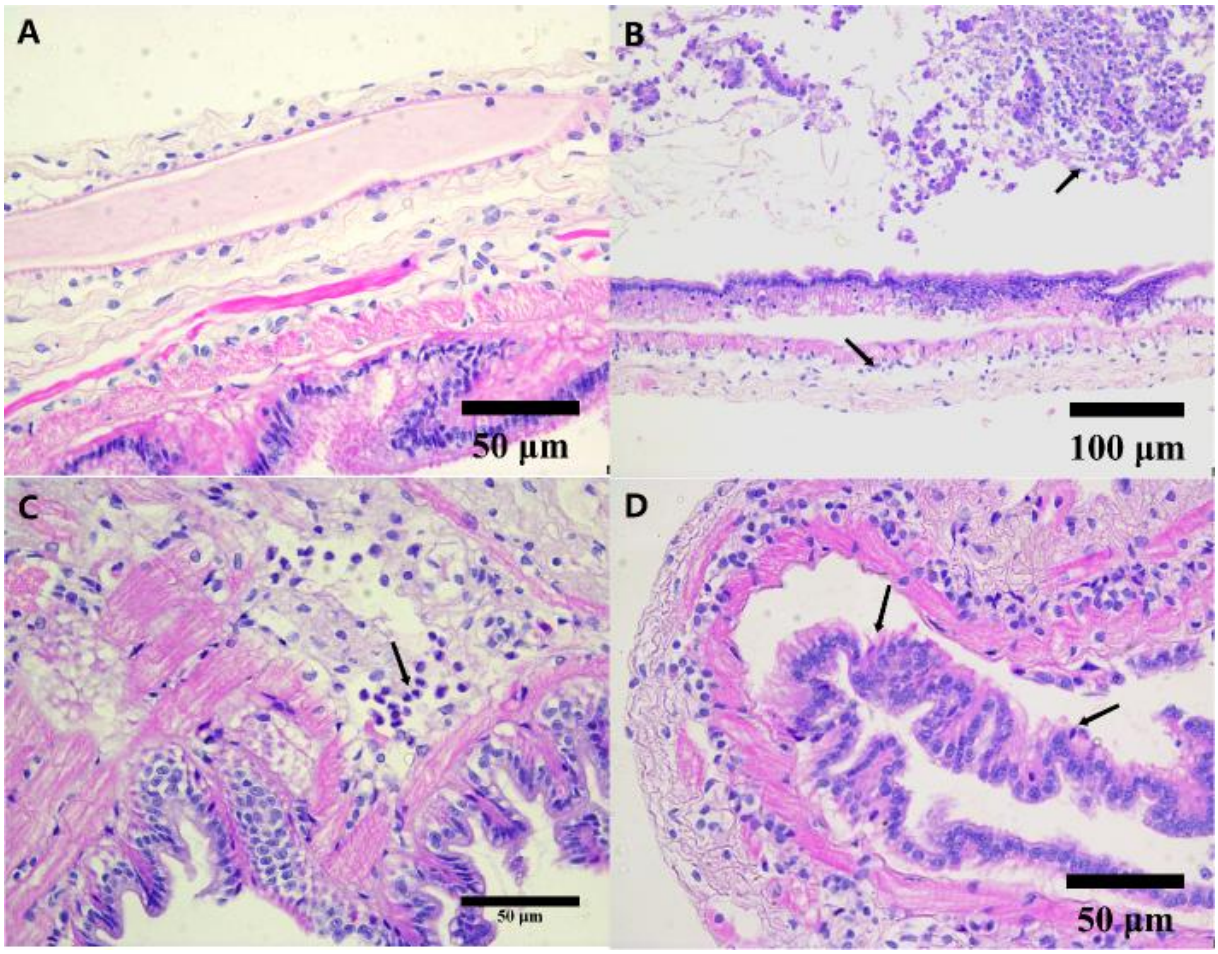

Fig. 7 Pathological sections of midgut of *P. vannamei.* (A) Normal midgut of shrimp. (B) shows the loads of *V. parahaemolyticus* were 1.9 copies/ng of midgut. (C) shows the loads of *V. parahaemolyticus* were 13.6 copies/ng of midgut. (D) shows the loads of *V. parahaemolyticus* were 49.7 copies/ng of midgut. The arrow refers to the cell or tissue lesions described

stellate lumen structure at their center. The stem cells at the distal end of the tubules differentiate into three types of epithelial cells: R cells, F cells, and B cells. (Figure 5A). In diseased shrimps, the epithelial cells of the hepatopancreas underwent morphological changes, becoming stellate and elongating towards the lumen, while a few cells exhibited nuclear swelling and a reduction in vacuoles. Additionally, there were occasional instances of hepatopancreatic epithelial cell shedding (Figure 5B, 2.4 copies/ng). As the load of *Vibrio* increases, many necrotic and exfoliated cells appear within the hepatopancreatic duct lumen. The originally clear and visible structure of the hepatic tubules is severely damaged, with the epithelial cell layer becoming atrophied and the number of functional cells reduced or difficult to discern (Figure 5C, 567.8 copies/ng). Under high loads of Vibrio, the proliferation of many *Vibrio* leads to severe destruction of hepatopancreatic tissue. Widespread ulceration and necrosis occur within the tissue, with the interstitial spaces filled with a large amount of necrotic material. In addition, pathological bleeding was observed, with a significant infiltration of blood cells and inflammatory cells in the damaged tissue (Figure 5D, 3938 copies/ng).

Pathological changes of muscle tissue

In the healthy shrimp, muscle is primarily composed of striated muscle tissue, with muscle fibers grouped into bundles. The spacing between the bundles is uniform, and they exhibit distinct striations in an orderly arrangement (Figure 6A). In diseased shrimps, the gaps between muscle fibers become enlarged, and the striated muscle undergoes rupture. Some muscle cells exhibit enlarged nuclei, and there is necrosis of certain cells (Figure 6B, 0.2 copies/ng). As the load of *Vibrio* increases, the extent of muscle fiber rupture worsens, and the amount of necrotic muscle tissue becomes more pronounced (Figure 6C, 3.4 copies/ng). Subsequently, extensive necrosis of muscle tissue occurs, with the dissociation of muscles becoming more severe. The striations between fibers largely disappear, making them difficult to discern. Most muscle fibers fragment into

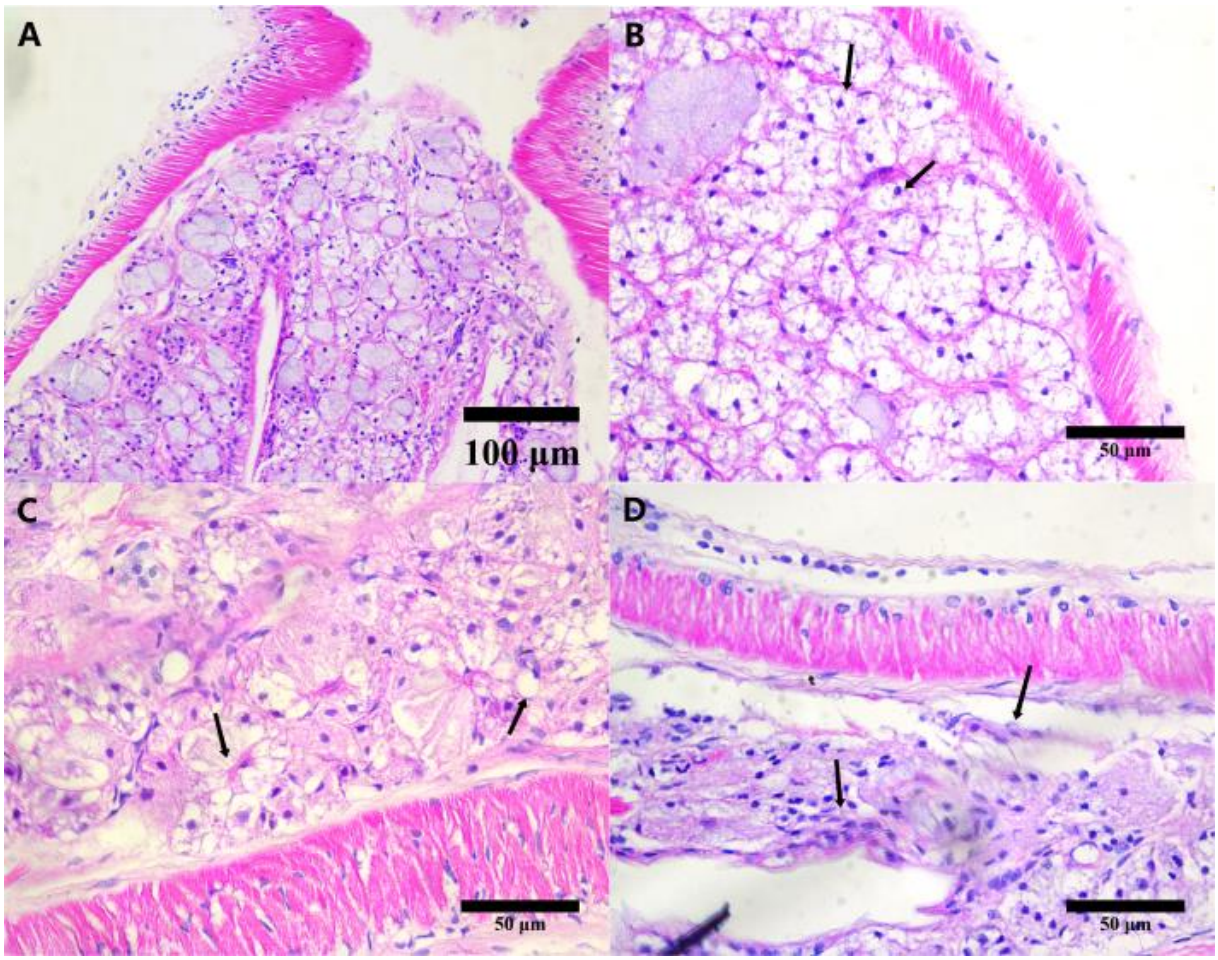

Fig. 8 Pathological sections of hindgut of *P. vannamei.* (A) Normal hindgut of shrimp. (B) shows the loads of *V. parahaemolyticus* were 1.1 copies/ng of hindgut. (C) shows the loads of *V. parahaemolyticus* were 6.7 copies/ng of hindgut. (D) shows the loads of *V. parahaemolyticus* were 62.9 copies/ng of hindgut. The arrow refers to the cell or tissue lesions described

pieces, leading to a disorganized dissociation of the muscle tissue structure. Necrotic cells are visible, sloughing off and accumulating among the tissues (Figure 6D, 8.6 copies/ng).

Pathological changes of midgut tissue

In the healthy shrimp, the midgut epithelial cells are closely arranged, forming villi that increase the absorptive surface area. The villi consist of a mucosal layer and a submucosal layer, with a clear boundary between them (Figure 7A). In diseased shrimps, the nuclei of the midgut epithelial cells exhibit pyknosis, and some cells have sloughed off, indicating that cellular structure and function are beginning to be compromised (Figure 7B, 1.9 copies/ng). As the load of *Vibrio* increases, the necrosis of midgut epithelial cells intensifies, with significant alterations in cell morphology. The gaps at the apical ends of the cells become enlarged, and the connections between cells are damaged, leading to a blurring of cell boundaries (Figure 7C, 13.6 copies/ng). The massive proliferation of *Vibrio* leads to more severe pathological damage. A separation occurs between the mucosal layer and the submucosal layer of the intestinal villi, with some villus cells sloughing off and tending to curl into balls. Many cells exhibit vacuolization internally, and there is widespread necrosis of the cell nuclei (Figure 7D, 49.7 copies/ng).

Pathological changes of hindgut tissue

In the healthy shrimp, the hindgut, as an important organ in the digestive system, is responsible for the absorption of water and electrolytes, as well as the excretion of waste. Its inner wall lacks villi and is instead covered by a chitinous epithelium (Figure 8A). In diseased shrimps, the epithelial cells of the hindgut also exhibit signs of nuclear pyknosis and cell necrosis, leading to sloughing off (Figure 8B, 1.1 copies/ng). As the load of *Vibrio* increases, the pathological changes in the hindgut epithelial cells become more severe, with the accumulation of sloughed-off necrotic cells and the occurrence of hollowing out and vacuolization in some cells (Figure 8C, 6.7 copies/ng). Under high loads of *Vibrio*, portions of the

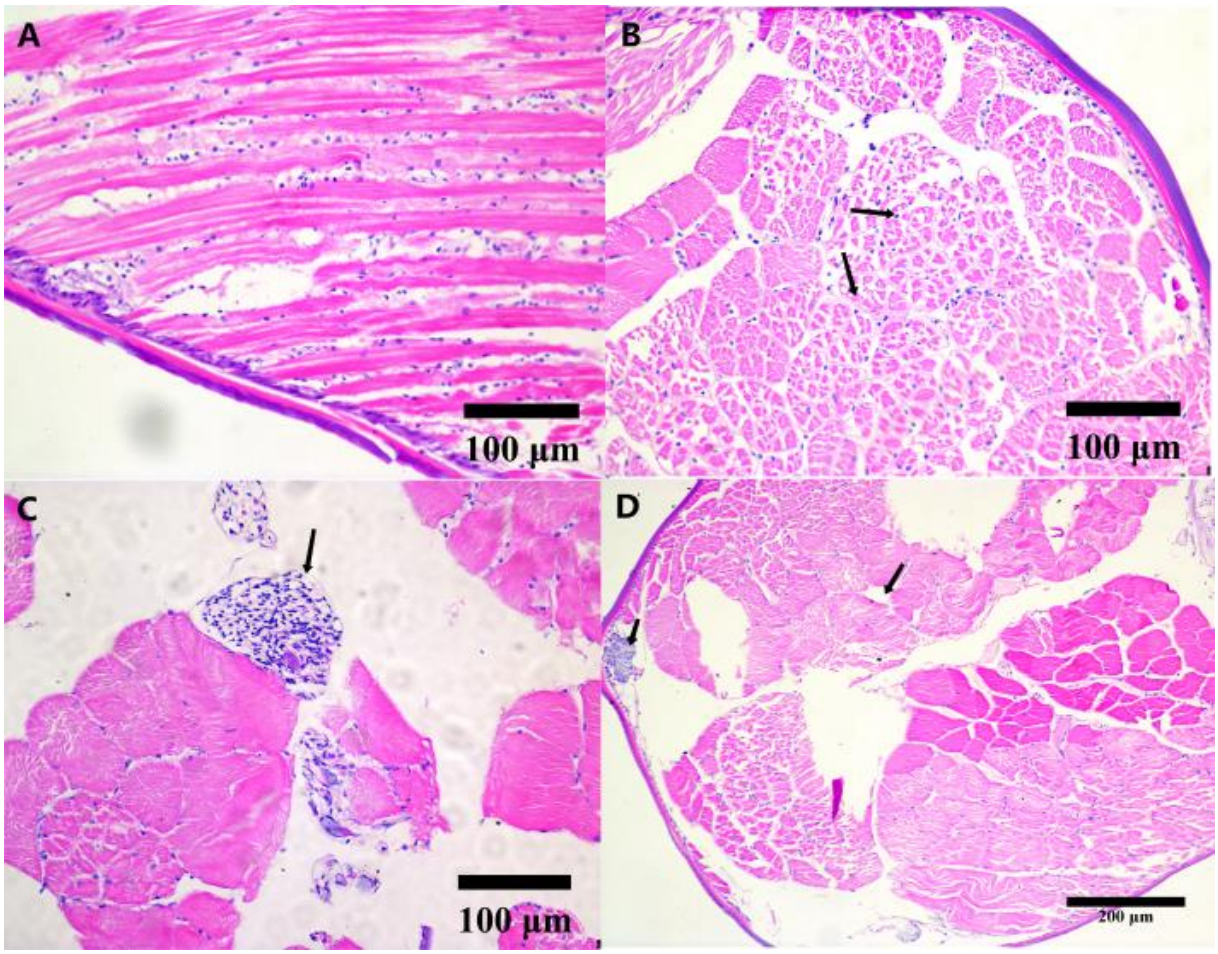

Fig. 9 Pathological sections of pleopod of *P. vannamei.* (A) Normal pleopod of shrimp. (B) shows the loads of *V. parahaemolyticus* were 2 copies/ng of pleopod. (C) shows the loads of *V. parahaemolyticus* were 32.8 copies/ng of pleopod. (D) shows the loads of *V. parahaemolyticus* were 66.2 copies/ng of pleopod. The arrow refers to the cell or tissue lesions described

mucosal epithelial layer and the submucosal tissue layer detach, leading to a disorganized arrangement of epithelial cells and the appearance of fractures in some of the epithelial villus layers (Figure 8D, 62.9 copies/ng).

Pathological changes of pleopod tissue

In the healthy shrimp, the surface of the pleopod is covered by a layer of epidermal cells. Beneath the epidermis lies the striated muscle, composed of elongated muscle fibers arranged in a tight and regular pattern, with distinct boundaries between the muscle bundles (Figure 9A). In diseased shrimps, the striated structure of the pleopod muscles is disrupted, with the dissociation of the muscle structure becoming irregular and the spaces between the muscle fibers increasing (Figure 9B, 2 copies/ng). As the load of *Vibrio* increases, the fracturing and dissociation of muscle fibers worsen, with a significant accumulation of necrotic material within the tissue, leading to necrosis in some muscle areas (Figure 9C, 32.8 copies/ng). Under high *Vibrio* loads, the muscle structure within the swimming leg tissues suffers extensive damage, with most muscle fibers undergoing fracturing and dissolution (Figure 9D, 66.2 copies/ng).

Discussion

The invasion of *V. parahaemolyticus* causing AHPND poses a significant threat to the shrimp farming industry (Lai *et al*., 2015; Choi *et al*., 2017). In recent years, the infection mechanisms of AHPND pathogens and methods for their detection have been extensively studied (Dangtip *et al*., 2015; Wangman *et al*., 2017; Xiao *et al*., 2017; Rizan *et al*., 2018; Aranguren Caro *et al*., 2020; Yu *et al*., 2020). Previous studies have shown that the *V. parahaemolyticus* causing AHPND primarily affects the digestive gland of shrimp, especially the hepatopancreas. As the infection progresses further, necrosis occurs in the hepatopancreatic tubules, with hemocyte infiltration triggering an inflammatory response and the formation of nodules (Nunan *et al*., 2014; Han *et al*., 2015b; Campa-Córdova *et al*.,

2017; Dong *et al*., 2017). However, research on the distribution and impact of *V. parahaemolyticus* in other tissues within the shrimp body is relatively scarce.

Infections by pathogens in aquatic environments tend to be systemic in aquatic animals. Research has indicated that upon exposing half-smooth tongue sole to varying concentrations of *Vibrio anguillarum*, a range of pathological alterations ensue. These encompass hepatic cell swelling within the liver, splenic red blood cell necrosis, head kidney hemorrhaging, as well as intestinal mucosa necrosis and exfoliation (Wang *et al*., 2023). Following a six-hour stimulation of *P. vannamei* with *V. parahaemolyticus*, the pathogenic agent has been identified within the gills, hepatopancreas, intestines, muscles, and hemolymph. The infectious agent persists in inducing pathological harm to these specified tissues (Khimmakthong and Sukkarun, 2017). In this study, we collected various tissue samples, including gills hepatopancreas including gills, heart, stomach, hepatopancreas, muscles, midgut, hindgut, and pleopod from survival, moribund, and dead shrimps for qPCR analysis. The qPCR results indicated that *V. parahaemolyticus* could infect the gills, heart, stomach, hepatopancreas, muscles, midgut, hindgut, and pleopod of shrimps and proliferate within these tissues as the infection progressed. Notably, in the hepatopancreatic samples, irrespective of whether the shrimp were alive, moribund, or dead, the qPCR positivity rates were very high. This finding suggests that the hepatopancreas is the primary target organ for *V. parahaemolyticus* infection, for the bacterial load in this tissue is significantly higher than in other tissues during the AHPND outbreak. Additionally, the pleopod and gills also exhibited high positivity rates and bacterial loads, indicating their potential value in disease diagnosis.

Histopathological observation is an important method for studying bacterial infections and their effects on hosts. Previous studies have shown that once *V. parahaemolyticus* is ingested through the mouth and enters the body of prawns, this bacterium can disrupt the balance of intestinal flora by competing for resources or secreting harmful metabolic products (Qi *et al*., 2017). This disturbance provides the pathogen with opportunities to proliferate and settle, and, along with the release of toxins, triggers inflammatory responses and immune reactions, leading to damage to cell gaps and cell connections, which in turn allows the toxins to reach the hepatopancreatic region (Ng *et al*., 2018). To understand the impact of *V. parahaemolyticus* on other tissues in shrimp, we conducted histopathological studies on the gills, heart, stomach, hepatopancreas, muscles, midgut, hindgut, and pleopod of diseased *P. vannamei*. The results showed that in the gills, the gill filaments were swollen with widened gill chambers, nuclear enlargement in cells, partial necrosis of gill filament cells, and disorganized arrangement of gill filaments. In the heart, muscles, and pleopod, there was muscle fiber breakage, disarray of myofibril arrangement, loss of striations, and widespread cellular degeneration and necrosis. In the intestinal tract of *P. vannamei*, the integrity of the intestinal epithelial cells and the intercellular connecting structures is fundamental to the physical barrier of the intestinal mucosa. In both the midgut and hindgut of infected shrimp, phenomena such as nuclear pyknosis and cell shedding were observed, with some intestinal villi experiencing separation between the mucosal layer and the lamina propria, disruption of intercellular connections, and blurring of cell boundaries. The pathological damage to the hepatopancreas was consistent with previous studies, exhibiting clear AHPND symptoms. Research indicates that after acute infection with *V. parahaemolyticus*, all tissues in shrimp can be affected by the bacteria, leading to a pathogen infection primarily characterized by degenerative necrosis of tissue cells. In the early stages of bacterial invasion into various tissues, partial cellular degeneration and a small amount of cell necrosis first occur, followed by destruction of the original tissue structure and further increase in the number of necrotic cells. Once the bacterial infection reaches a certain level, severe pathological damages, and degrees of inflammation, such as partial necrosis and structural dissociation, occur across different tissues.

In summary, this study combined molecular biology and histopathology to investigate the relationship between tissue bacterial load and pathological damage changes in *P. vannamei* infected with *V. parahaemolyticus* causing AHPND. There is a high correlation between the bacterial load of *V. parahaemolyticus* in the tissues and the pathological damage. The analysis indicates that after infection with the bacteria, the hepatopancreas, gills, and pleopod are all susceptible tissues for AHPND.

Acknowledgements

This research is supported by the PI Project of Southern Marine Science and Engineering Guangdong Laboratory (Guangzhou) (GML20220018).

References

Ananda Raja R, Sridhar R, Balachandran C, Palanisammi A, Ramesh S, Nagarajan K. Pathogenicity profile of *Vibrio parahaemolyticus* in farmed Pacific white shrimp, *Penaeus vannamei*. Fish Shell. Immunol. 67: 368-381, 2017.

Aranguren Caro LF, Mai HN, Kanrar S, Cruz-Flores R, Dhar AK. A Mutant of *Vibrio parahaemolyticus* pirAB(VP) (+) That Carries Binary Toxin Genes but Does Not Cause Acute Hepatopancreatic Necrosis Disease. Microorganisms 8: 1549, 2020.

Campa-Córdova AI, León-Gallo AF, Romero-Maldonado A, Ibarra-Serrano AC, Rosales-Mendoza S, Hirono I, *et al*. Recombinant PirA-like toxin protects shrimp against challenge with *Vibrio parahaemolyticus*, the aetiological agent of acute hepatopancreatic necrosis disease. J. Fish Dis. 40: 1725-1729, 2017.

Choi M, Stevens AM, Smith SA, Taylor DP, Kuhn DD. Strain and dose infectivity of *Vibrio parahaemolyticus*: the causative agent of early

mortality syndrome in shrimp. Aqua. Res. 48: 3719-3727, 2017.

Cruz-Flores R, Mai HN, Dhar AK. Multiplex SYBR Green and duplex TaqMan real-time PCR assays for the detection of *Photorhabdus* Insect-Related (Pir) toxin genes pirA and pirB. Mol. Cell. Probes. 43: 20-28, 2019.

Dangtip S, Sirikharin R, Sanguanrut P, Thitamadee S, Sritunyalucksana K, Taengchaiyaphum S, Mavichak R, *et al*. AP4 method for two-tube nested PCR detection of AHPND isolates of *Vibrio parahaemolyticus*. Aqua. Rep. 2: 158-162, 2015.

de la Peña LD, Cabillon NA, Catedral DD, Amar EC, Usero RC, Monotilla W D, et al. Acute hepatopancreatic necrosis disease (AHPND) outbreaks in *Penaeus vannamei* and *P. monodon* cultured in the Philippines. Dis. Aquat. Organ.116: 251-254, 2015.

Dhar AK, Piamsomboon P, Aranguren Caro LF, Kanrar S, Adami R, Juan YS. First report of acute hepatopancreatic necrosis disease (AHPND) occurring in the USA. Dis. Aqua. Organ.132: 241-247, 2019.

Dong X, Bi D, Wang H, Zou P, Xie G, Wan X, *et al*. PirAB(vp) -Bearing *Vibrio parahaemolyticus* and *Vibrio campbellii* Pathogens Isolated from the Same AHPND-Affected Pond Possess Highly Similar Pathogenic Plasmids. Front. Microbiol. 8: 1859, 2017.

Han JE, Tang KFJ, Pantoja CR, White BL, Lightner DV. qPCR assay for detecting and quantifying a virulence plasmid in acute hepatopancreatic necrosis disease (AHPND) due to pathogenic *Vibrio parahaemolyticus*. Aquaculture. 442: 12-15, 2015a.

Han JE, Tang KF, Tran LH, Lightner DV. Photorhabdus insect-related (Pir) toxin-like genes in a plasmid of *Vibrio parahaemolyticus*, the causative agent of acute hepatopancreatic necrosis disease (AHPND) of shrimp. Dis. Aqua. Organ.113: 33-40, 2015b.

Hong X, Lu L, Xu D. Progress in research on acute hepatopancreatic necrosis disease (AHPND). Aqua. Int. 24: 577-593, 2016.

Hu F, Gong X, Hu J, Bao Z, Wang M. RNA interference confirmed a close association of CYP, ApD, and UCH with the function of CpG ODNs in *Litopenaeus vannamei*. Aquaculture. 585: 740707, 2024.

Khimmakthong U, Sukkarun P. The spread of *Vibrio parahaemolyticus* in tissues of the Pacific white shrimp *Litopenaeus vannamei* analyzed by PCR and histopathology. Micro. Pathog. 113: 107-112, 2017.

Kongrueng J, Tansila N, Mitraparp-arthorn P, Nishibuchi M, Vora GJ, Vuddhakul V. LAMP assay to detect *Vibrio parahaemolyticus* causing acute hepatopancreatic necrosis disease in shrimp. Aqua. Int. 23: 1179-1188, 2015.

Lai HC, Ng TH, Ando M, Lee CT, Chen IT, Chuang JC, *et al*. Pathogenesis of acute hepatopancreatic necrosis disease (AHPND) in shrimp. Fish Shellfish. Immunol. 47: 1006-1014, 2015.

Lee CT, Chen IT, Yang YT, Ko TP, Huang YT, Huang JY, et al. The opportunistic marine pathogen *Vibrio parahaemolyticus* becomes virulent by acquiring a plasmid that expresses a deadly toxin. Proc. Natl. Acad. Sci. 112: 10798-10803, 2015.

Lee D, Yu YB, Choi JH, Jo AH, Hong SM, Kang JC, *et al*. Viral Shrimp Diseases Listed by the OIE: A Review. Viruses. 14: 585, 2022.

Li JB, Hu JJ, Bao ZM, Wang MQ. Rapid and sensitive detection of Taura syndrome virus (TSV) in shrimp based on an isothermal enzymatic recombinase amplification (ERA) assay. Aqua Int, 32: 6211-6225. 2024.

Li JB, Wang Y, Hu JJ, Bao ZM, Wang MQ. An isothermal enzymatic recombinase amplification (ERA) assay for rapid and accurate detection of *Enterocytozoon hepatopenaei* infection in shrimp. J. Invertebr. Pathol. 197: 107895, 2023.

Li S, Zhang K, Du W, Li F. Two Independently Comparative Transcriptome Analyses of Hemocytes Provide New Insights into Understanding the Disease-Resistant Characteristics of Shrimp against *Vibrio* Infection. Biology.12: 977, 2023.

Lightner DV, Hasson KW, White BL, Redman RM. Chronic toxicity and histopathological studies with Benlate, a commercial grade of benomyl, in *Penaeus vannamei* (Crustacea: Decapoda). Aqua. Toxi. 34: 105-118. 1996.

Liu K, Zhang L, Yang J, Zeng Q, Hu J, Bao Z, *et al*. An enzymatic recombinase amplification assay combined with CRISPR-Cas12a for the rapid detection of acute hepatopancreatic necrosis disease in shrimp *Penaeus vannamei*. Aqua. Inter. 32: 7695-7718. 2024.

Martin GG, Rubin N, Swanson E. *Vibrio parahaemolyticus* and *V. harveyi* cause detachment of the epithelium from the midgut trunk of the penaeid shrimp *Sicyonia ingentis*. Dis. Aqua. Organ. 60: 21-29, 2004.

Ng TH, Lu CW, Lin SS, Chang CC, Tran LH, Chang WC, *et al*. The Rho signalling pathway mediates the pathogenicity of AHPND-causing *V. parahaemolyticus* in shrimp. Cell Microbiol. 20: e12849, 2018.

Nunan L, Lightner D, Pantoja C, Gomez-Jimenez S. Detection of acute hepatopancreatic necrosis disease (AHPND) in Mexico. Dis. Aqua. Organ. 111: 81-86, 2014.

Qi CC, Wang L, Liu M, Jiang KY, Wang MQ, Zhao W, *et al*. Transcriptomic and morphological analyses of *Litopenaeus vannamei* intestinal barrier in response to *Vibrio paraheamolyticus* infection reveals immune response signatures and structural disruption. Fish Shell. Immunol. 70: 437-450, 2017.

Rizan N, Yew CY, Niknam MR, Krishnasamy J, Bhassu S, Hong GZ, *et al*. Electronic Properties of Synthetic Shrimp Pathogens-derived DNA Schottky Diodes. Sci. Rep. 8: 896, 2018.

Tran L, Nunan L, Redman RM, Mohney LL, Pantoja CR, Fitzsimmons K, *et al*. Determination of the infectious nature of the agent of acute hepatopancreatic necrosis syndrome affecting

penaeid shrimp. Dis. Aqua. Organ. 105: 45-55, 2013.

Wang W, Xu Q, Zang S, Liu X, Liu H, Li Z, *et al*. Inflammatory reaction and immune response of half-smooth tongue sole (*Cynoglossus semilaevis*) after infection with *Vibrio anguillarum*. Fish Shellfish. Immunol. 141: 109043, 2023.

Wangman P, Chaivisuthangkura P, Sritunyalucksana K, Taengchaiyaphum S, Senapin S, Pengsuk C, *et al*. Development of monoclonal antibodies specific to ToxA and ToxB of *Vibrio parahaemolyticus* that cause acute hepatopancreatic necrosis disease (AHPND). Aquaculture. 474: 75-81, 2017.

Xiao J, Liu L, Ke Y, Li X, Liu Y, Pan Y, *et al*. Shrimp AHPND-causing plasmids encoding the PirAB toxins as mediated by pirAB-Tn903 are prevalent in various *Vibrio* species. Sci. Rep.7: 42177, 2017.

Xu YJ, Wang Y, Hu JJ, Bao ZM, Wang MQ. Development and visualization improvement for the rapid detection of Decapod iridescent virus 1 (DIV1) in *Penaeus vannamei* based on an isothermal recombinase polymerase amplification assay. Viruses, 14: 2752, 2022.

Xu YJ, Wang Y, Hu JJ, Bao ZM, Wang MQ. The development of a novel quantitative assay for the detection of convert mortality nodavirus (CMNV) in *Litopenaeus vannamei*. Aquaculture, 577: 739923, 2023.

Yu LH, Teh CSJ, Yap KP, Thong KL. Diagnostic approaches and contribution of next-generation sequencing technologies in genomic investigation of *Vibrio parahaemolyticus* that caused acute hepatopancreatic necrosis disease (AHPND). Aqua. Int. 28: 2547-2559, 2020.

Zhang L, Liu KX, Liu MR, Hu JJ, Bao ZM, Wang MQ. Development of a real-time enzymatic recombinase amplification assay for rapid detection of infectious hypodermal and hematopoietic necrosis virus (IHHNV) in shrimp *Penaeus vannamei*. J. Invertebr. Pathol. 201: 108024. 2023a

Zhang L. Wang Y, Hu JJ, Bao ZM, Wang MQ. Rapid detection of white spot syndrome virus in *Penaeus vannamei* based on real-time enzymatic recombinase amplification. Aquaculture. 566: 739196, 2023b.

Zhang L. Wang Y, Hu JJ, Bao ZM, Wang MQ. Development of a multiplex real-time enzymatic recombinase amplification assay for differentiation of yellow head virus genotype 1 and 2 in *Penaeus vannamei*. Aquaculture. 582: 740564, 2024a.

Zhang L, Zhou Q, Liu JJ, Liu MR, Hu JJ, Bao ZM, *et al*. Development of recombinase amplification assays for the rapid detection of infectious myonecrosis virus. J. Invertebr. Pathol. 205: 108143. 2024b

Zhang T, Zhang M, Zhang X, Fang HH. Tetracycline resistance genes and tetracycline resistant lactose-fermenting Enterobacteriaceae in activated sludge of sewage treatment plants. Envir. Sci. Technol. 43: 3455-3460. 2009.

Zhou QQ, Wang Y, Hu JJ, Bao ZM, Wang MQ. Development of a real-time enzymatic recombinase amplification assay (RT-ERA) and an ERA combined with lateral flow dipsticks (LFD) assay (ERA-LFD) for rapid detection of acute hepatopancreatic necrosis disease (AHPND) in shrimp *Penaeus vannamei*. Aquaculture. 566: 739205, 2023.